Langmuir

Article

pubs.acs.org/Langmuir

Covalent Layer-by-Layer Assembly of Redox-Active Polymer Multilayers

Xueling Feng,[†] Aysegul Cumurcu,[†] Xiaofeng Sui,[†] Jing Song,[‡] Mark A. Hempenius,[†] and G. Julius Vancso*,[†]

[†]Department of Materials Science and Technology of Polymers, University of Twente, MESA+ Institute for Nanotechnology, P.O. Box 217, 7500 AE Enschede, The Netherlands

[‡]Institute of Materials Research and Engineering, A*STAR Singapore, Research Link 3, 117602 Singapore

Supporting Information

ABSTRACT: Poly(ferrocenyl(3-bromopropyl)methylsilane) and poly(ethylene imine) are employed in a layer-by-layer deposition process to form covalently connected, redox-active multilayer thin films by means of an amine alkylation reaction. The stepwise buildup of these multilayers on silicon, ITO, and quartz substrates was monitored by UV−vis absorption spectroscopy, Fourier transform infrared spectroscopy (FTIR), static contact angle measurements, surface plasmon resonance (SPR), atomic force microscopy, ellipsometry, and cyclic voltammetry, which provide evidence for a linear increase in multilayer thickness with the number of deposited bilayers. Upon oxidation and reduction, these covalently interconnected layers do not disassemble, in contrast to poly(ferrocenylsilane) (PFS) layers featuring similar backbone structures that are held together by electrostatic forces. The PFS/PEI multilayers are effective for the electrochemical sensing of ascorbic acid and hydrogen peroxide and show improved sensing performance at higher bilayer numbers. These covalently linked layers are readily derivatized further and can therefore be regarded as a versatile platform for creating robust, tailorable, redox-active interfaces with applications in sensing and biofuel cells.

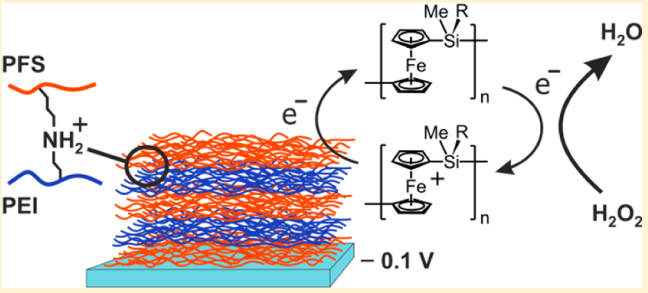

INTRODUCTION

The modification of electrode surfaces with electroactive species has been a topic of major interest in the past decades because of the tremendous application potential of functionalized electrodes in the areas of ion recognition,[1] electrocatalysis,[2] amperometric biosensors,[3] biofuel cells,[4] and molecular electronics.[5] The surface-anchoring of thiol- or disulfide-containing redox-active molecules onto gold surfaces has resulted in self-assembled monolayers (SAMs) and mixed SAMs.[6] In addition to small molecules, polymeric redox-active species have been widely employed to create chemically modified electrodes.[7] Typical examples include poly(vinylferrocene) and polymerized $Ru(vbpy)_3^{2+}$, polymers consisting of poly(allylamine),[8] poly(ethylene imine),[3a] or poly(methacrylate)[9] backbones with pendant redox-active units, and conducting polymers such as poly(pyrrole) and poly(thiophene).[10]

Because many applications require the incorporation of additional functions such as biorecognition elements within the redox-active layer, it is desirable to construct the redox-active film in a stepwise manner. A highly versatile approach for the stepwise construction of thin polymer films with controlled composition and thickness is the electrostatic layer-by-layer (LbL) deposition process.[11] Initially, LbL-related research was focused primarily on the use of commercially available polyelectrolytes for constructing thin films.[12] Subsequent work demonstrated that many other materials can also be used in the preparation of films. Furthermore, in addition to electrostatics, various driving forces for film assembly were exploited, including hydrogen bonding,[13,14] DNA hybridization,[15,16] sequential chemical reactions,[17−20] metal coordination,[21] and ligand−receptor interactions,[22] implying that the LbL method is not restricted to charged materials. The use of covalent bonds to assemble LbL films is an emerging area of interest. Covalent connections between deposited chains prevent layer disassembly, which may occur for electrostatically assembled multilayers with changes in pH or ionic strength.

A fascinating class of redox-active materials, poly(ferrocenylsilanes) (PFSs),[23] composed of alternating ferrocene and silane units in their main chain combine a high density of redox centers with excellent processability and possess redox characteristics[24] suitable for the electrochemical detection of biological analytes. Several reports have appeared on the formation of thin PFS films on electrodes and other surfaces using the layer-by-layer deposition of PFS polyions.[25,26] Multilayered organometallic thin films, held together only by

Special Issue: Interfacial Nanoarchitectonics

Received: November 11, 2012
Revised: January 12, 2013
Published: January 13, 2013

electrostatic interactions, were used for the redox-controlled release of molecular payloads stored within the films.[27] PFS films can also be anchored on solid substrates through covalent bonds. We recently reported the fabrication of a covalently immobilized poly(ferrocenylsilane) film on a gold electrode using reactive side groups of the PFS chains for surface anchoring.[28,29] The stable, ultrathin redox-active films resulting from this "grafting-to" approach[30] were successfully used in the electrochemical sensing of ascorbic acid. These layers are readily derivatized further and can therefore be regarded as a versatile platform for creating robust, tailorable redox-active interfaces. Here we extend this grafting-to method to a covalent LbL deposition process for the sequential buildup of covalently interconnected PFS layers on ITO and Si substrates using an amine alkylation reaction between PFS bromopropyl side groups and poly(ethylene imine). In contrast to the widely explored electrostatic LbL deposition process, LbL processes where covalent bonds are formed between layers are relatively rare.[11] Very few examples exist of covalently constructed LbL films involving a polymer with pendant redox units,[31] and to our knowledge, there are no accounts of LbL films based on covalently linked redox-active polymers with skeletal redox units. We monitored multilayer growth by UV−vis spectroscopy, static contact angle (SCA) measurements, surface plasmon resonance (SPR) spectroscopy, atomic force microscopy (AFM), and cyclic voltammetry (CV). The performance of these stable, ultrathin redox-active films in the electrochemical sensing of hydrogen peroxide[32] as a function of the number of bilayers is discussed.

EXPERIMENTAL SECTION

Materials. Poly(ferrocenyl(3-bromopropyl)methylsilane) (**1**) (M_w = 3.93 × 10^5 g/mol, M_n = 1.61 × 10^5 g/mol, M_w/M_n = 2.4) was synthesized according to established procedures.[33] (3-Aminopropyl)-trimethoxysilane (97%), poly(ethylene imine) (branched, average M_n ≈ 1.00 × 10^4 g/mol by GPC, average M_w ≈ 2.50 × 10^4 g/mol by LS according to the supplier, ≤1% water), cysteamine (≥98.0%), and sodium perchlorate (≥98.0%) were obtained from Sigma-Aldrich and used as received. Tetrahydrofuran (THF) was purified by distillation from sodium benzophenone under argon. All water used in the experiments was Milli-Q grade. Hydrogen peroxide (for analysis, 35 wt % solution in water) was obtained from Acros Organics.

Formation of (3-Aminopropyl)trimethoxysilane SAMs. Indium tin oxide (ITO, for CV measurements), silicon (for AFM and ellipsometry measurements), and quartz (for UV−vis spectroscopy) substrates were first cleaned with piranha solution (base or acid) and then rinsed extensively with water and ethanol. (***Caution!*** *Piranha solution reacts violently with many organic materials and should be handled with great care.*) The dried substrates were placed at the bottom of a desiccator around a vial containing 100 μL of (3-aminopropyl)trimethoxysilane. The desiccator was then evacuated with a rotary vane pump for 10 min and subsequently closed. Vapor-phase silanization was allowed to proceed overnight. The substrates were then rinsed with toluene and ethanol, dried in a stream of N_2, and immediately used for LbL assembly.

Formation of Cysteamine SAMs. Gold substrates (for SPR measurements) were cleaned with piranha solution and extensively rinsed with water, ethanol, and dichloromethane. Cysteamine SAMs were prepared by immersing gold substrates in ethanol solutions, containing 1 wt % cysteamine, for 16 h. The substrates were then rinsed with ethanol, dried in a stream of N_2, and immediately used for LbL assembly.

Multilayer Fabrication. The amine-modified substrates were alternately immersed in solutions of PFS **1** (in 4:1 v/v THF/DMSO, 2 mg/mL) and PEI (in 4:1 v/v THF/DMSO, 2 mg/mL) for 30 min and after each deposition step rinsed with THF (PFS **1** outer layer) or Milli-Q water (PEI outer layer), immersed in pure THF or Milli-Q water for 2 min, rinsed with ethanol, and dried in a stream of nitrogen.

UV−Vis Spectroscopy. UV−vis absorption spectra were recorded using a Perkin-Elmer Lambda 850 UV−vis spectrophotometer.

Fourier Transform Infrared (FTIR) Measurements. FTIR spectra were obtained using a Bio-Rad FTS 575C spectrometer. A background spectrum was obtained by scanning a clean silicon substrate.

Static Contact Angle (SCA) Measurements. SCA measurements were performed by the sessile drop technique using an optical contact angle device equipped with an electronic syringe unit (OCA15, Dataphysics, Germany). The sessile drop was deposited onto the surface of the materials with the syringe, and the drop contour was fitted by the Young−Laplace method. At least three different measurements of each sample were performed.

Ellipsometry Measurements. An M-2000X variable-angle spectroscopic ellipsometer (J.A. Woollam Co., Lincoln, NE, USA) system was used. Measurements were performed at wavelengths ranging from 210 to 1000 nm (1.25−5.85 eV) at three angles (65, 70, and 75°). The spot size of the probing light had a diameter of 2 mm. Data fitting was performed with a commercial software package (Complete EASE v.4.41) supplied with the M-2000X system. The thickness of the multilayer films deposited on silicon substrates was determined, assuming simple Cauchy dispersions.

Surface Plasmon Resonance (SPR) Measurements. SPR spectra were collected by using a Multiskop instrument (Optrel, Germany) equipped with a 632.8 nm He−Ne laser. An SPR chip (gold thickness of 50 nm, XanTec Bioanalytics, Düsseldorf, Germany) and a 90° LaSFN9 prism (Hellma Optik, Jena, Germany) with a refractive index of 1.845 (at λ = 632.8 nm) were assembled in the Kretschmann configuration. The SPR chip was optically matched to the base of the prism using a refractive index matching oil (Series B, Cargille Laboratories, Cedar Grove, NJ, USA). The intensity of the reflected light as a function of the angle of incidence was recorded. The reflected intensity showed a sharp minimum at a resonance angle that depends on the precise architecture of the interface. The measured angular reflectivity curves were fitted using the Optrel GbR surface plasmon data evaluation and simulation program (v. 2.1). Layer thicknesses were determined by nonlinear least-squares fitting to a layer model using Fresnel theory and refractive index values of 1.57 for PFS[34] and 1.50 for PEI.[35]

Atomic Force Microscopy (AFM) Measurements. AFM measurements were performed with a Dimension D3100 AFM equipped with a NanoScope IVa controller (Bruker, Santa Barbara, CA, USA) in tapping mode using commercially available silicon cantilevers (PointProbe Plus silicon probes, PPP-NCH, Nanosensors, Neuchâtel, Switzerland) to measure the thickness and surface morphology of the grafted layers.

Electrochemical Measurements. Electrochemical measurements were carried out with multilayers on ITO substrates in aqueous $NaClO_4$ (0.1 M) using an Autolab PGSTAT 10 electrochemical workstation. Cyclic voltammograms were recorded between −0.1 and +0.9 V at various scan rates using a Ag/AgCl reference electrode and a Pt counter electrode.

RESULTS AND DISCUSSION

The redox-active component employed in the LbL construction of the redox-active multilayers, poly(ferrocenyl(3-bromopropyl)methylferrocene) **1**, was synthesized according to a published procedure.[33] High-molar-mass, branched poly(ethylene imine) (PEI) was used to interconnect the PFS chains via amine alkylation reactions. To verify sufficient reactivity, PFS **1** and PEI were mixed in the deposition medium, 4:1 v/v THF/DMSO. A precipitate formed within 10 min (Figure S1, Supporting Information). Multilayers of PFS **1** and PEI were fabricated on various substrates to determine if well-defined film growth occurred. An alternate adsorption of PFS **1** and PEI was conducted as depicted in Scheme 1. First,

Scheme 1. Schematic Representation of PFS/PEI Multilayer Fabrication on Amine-Functionalized Substrates

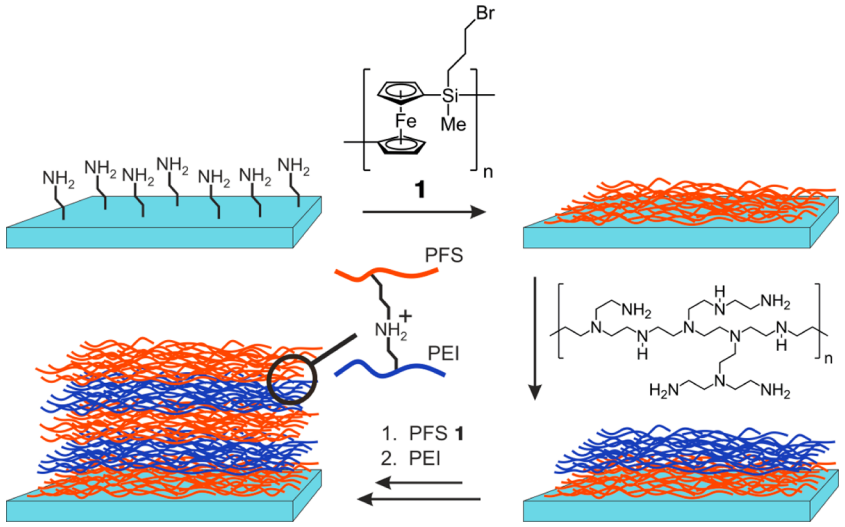

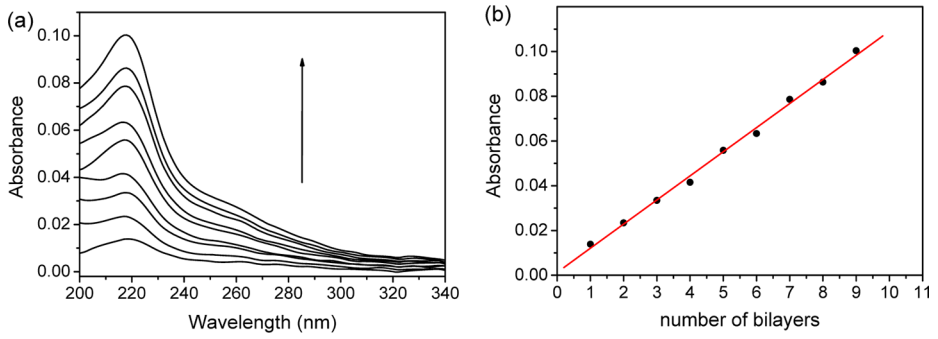

Figure 1. (a) UV−vis absorption spectra of sequentially adsorbed layers of PFS **1** and PEI deposited from 4:1 v/v THF/DMSO on quartz. (b) Absorption at λ = 216 nm as a function of the number of bilayers.

silicon or ITO substrates were treated with (3-aminopropyl)-trimethoxysilane to create an amine-terminated surface for the attachment of PFS **1**. The substrate was subsequently immersed in a 2 mg/mL solution of **1** in THF/DMSO, rinsed, and immersed in a PEI solution of the same concentration.

The sequential buildup of PFS/PEI multilayers on quartz slides was monitored by UV−vis spectroscopy. After each deposited bilayer, a spectrum was recorded. Figure 1 shows the increase in the absorbance at λ = 216 nm associated with the intense ligand-to-metal charge-transfer transition (LMCT)[36] characteristic of PFS as a function of the number of bilayers. A linear increase in this absorbance with the number of PFS/PEI bilayers was observed, which is indicative of a well-defined deposition process. Interestingly, the linear increase in absorbance is already observed in the first few bilayers, and the fitted line passes through the origin. Thus, this deposition process does not show a transient for the first few layers, as commonly observed for electrostatic LbL depositions where the substrate influences the number of adsorbed chains.[37]

FTIR was used to obtain further information on bonds formed within the PFS/PEI multilayer. Figure S2 (Supporting Information) shows the FTIR spectra of PEI, PFS **1**, and $(PFS/PEI)_8$-PFS. In the spectrum of PEI, the band at 1578 cm^{-1} is associated with the N−H bending vibration of primary amines.[38] The absorption at 1120 cm^{-1} belongs to the C−N stretching of secondary amine groups.[38] In the spectrum of the $(PFS/PEI)_8$-PFS multilayer, the band at 1578 cm^{-1} became weaker and a strong absorption appeared at 1110 cm^{-1}, indicating that primary amine groups changed to secondary amine groups.

The layer-by-layer buildup on silicon substrates was monitored by static contact angle measurements. It is known that the outermost layer of LbL-deposited films governs the wettability of multilayer assemblies.[39] Because hydrophobic (PFS) and hydrophilic (PEI) building blocks are used, successful multilayer growth should result in alternating contact angle values. As layers were added, contact angles alternated between 63 ± 2° for PFS outer layers and 45 ± 2° for PEI outer layers (Table 1), providing clear evidence for the stepwise LbL assembly of the PFS/PEI multilayer films. The obtained contact angles for PEI outer layers matched the literature values for PEI-based multilayers.[40] The covalent layer-by-layer assembly process was also gauged by surface plasmon spectroscopy (SPR). Figure 2 shows the various reflectivity curves obtained during the LbL deposition of PFS **1** and PEI.

Table 1. Static Contact Angles Measured During PFS/PEI Multilayer Buildup

	PFS 1 (deg)	PEI (deg)
bilayer 1	67 ± 2	30 ± 2
bilayer 2	65 ± 2	42 ± 2
bilayer 3	60 ± 2	45 ± 2
bilayer 4	63 ± 2	45 ± 2

dx.doi.org/10.1021/la304498g | *Langmuir* 2013, 29, 7257−7265

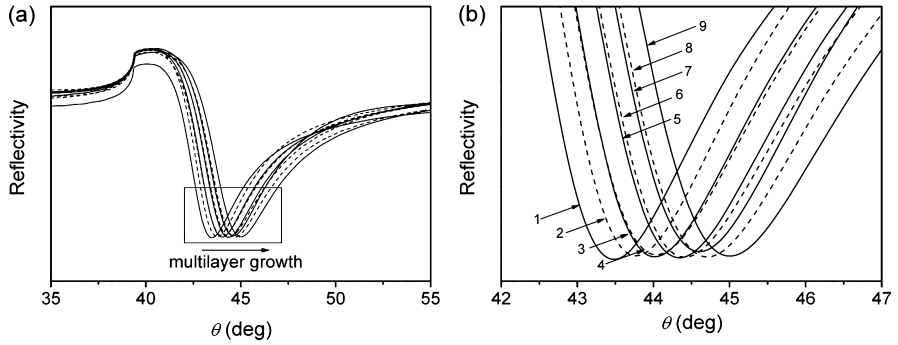

Figure 2. (a) Reflected intensity as a function of the angle-of-incidence scan (θ) plot showing the assembly of the multilayered structure on the Au substrate. (b) Expanded view of the SPR spectra in the range of the reflectivity minimum. The various reflectivity curves correspond to (1) the amine-functionalized Au surface, (2) $(PFS)_1$, (3) $(PFS/PEI)_1$, (4) $(PFS/PEI)_1$-PFS, (5) $(PFS/PEI)_2$, (6) $(PFS/PEI)_2$-PFS, (7) $(PFS/PEI)_3$, (8) $(PFS/PEI)_3$-PFS, and (9) $(PFS/PEI)_4$.

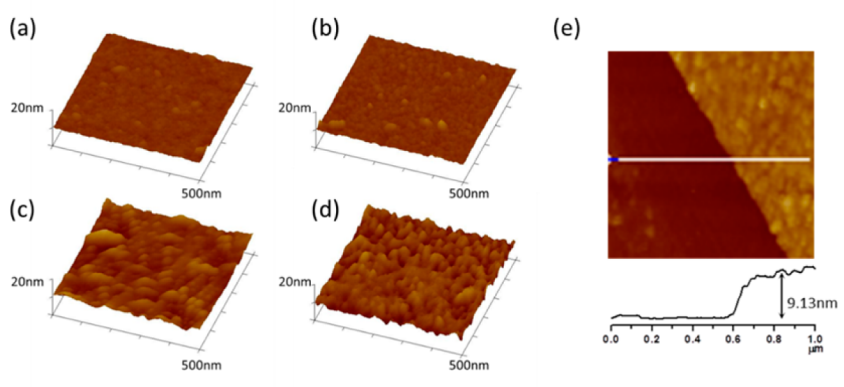

Figure 3. Tapping-mode AFM images of (a) an amine-functional Si substrate after attaching PFS **1** (i.e., $(PFS)_1$), (b) $(PFS/PEI)_1$, (c) $(PFS/PEI)_4$-PFS, and (d) $(PFS/PEI)_8$-PFS, scanned over a 0.5 × 0.5 μm^2 area. (e) AFM image and cross-sectional height profile of a $(PFS/PEI)_8$-PFS film assembled on a Si substrate. The rms roughness values for these layers are (a) 0.6, (b) 0.7, (c) 1.4, and (d) 1.9 nm.

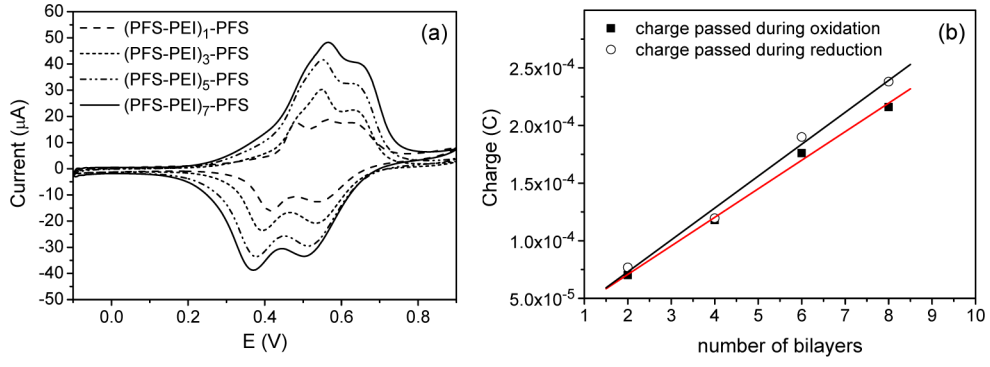

Figure 4. (a) Cyclic voltammograms for PFS/PEI multilayers on ITO substrates in a 0.1 M $NaClO_4$ aqueous electrolyte, with a Ag/AgCl reference electrode and a Pt counter electrode. The scan rate is 50 mV/s. (b) Charge passed during oxidation/reduction for varying numbers of bilayers. R_{ox} = 0.993 and R_{re} = 0.988.

SPR responses originate from refractive index changes, and the shifts in the minimum of the angular θ scans of reflected intensity signify the sequential assembly of the different building blocks into the layered architecture. A Fresnel fit to the resonance curve of bare and coated Au surfaces gave optical thicknesses of the multilayer films. On the basis of known refractive indices of the film components (RI_{PFS} = 1.57,[34] RI_{PEI} = 1.50[35]) a bilayer thickness of 1.4 nm was found for the multilayer films.

Figure 3 shows the surface morphology of PFS/PEI films as a function of the number of bilayers, measured by tapping mode AFM, and the film height of a $(PFS/PEI)_8$-PFS multilayer on silicon substrates. The rms roughness of the multilayer over a scanned area of 0.5 × 0.5 μm^2 increased with the number of bilayers. For a single layer of PFS **1** attached to an amine-functional Si substrate, $(PFS)_1$, the value of the rms roughness was 0.6 nm, 0.7 nm for $(PFS/PEI)_1$, 1.4 nm for $(PFS/PEI)_4$-PFS, and 1.9 nm for $(PFS/PEI)_8$-PFS. To demonstrate the homogeneity of these films, scans were also performed over

dx.doi.org/10.1021/la304498g | Langmuir 2013, 29, 7257−7265

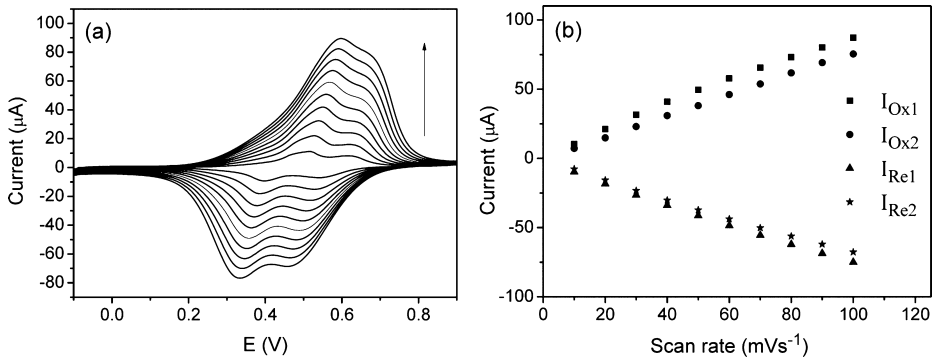

Figure 5. (a) Cyclic voltammograms of a $(PFS/PEI)_8$-PFS multilayer on ITO at various scan rates in 0.1 M $NaClO_4$, with a Ag/AgCl reference electrode, and a Pt counter electrode. The scan rate was varied from 10 to 100 mV/s, and the potential range applied was −0.1 to 0.9 V vs Ag/AgCl. (b) Dependence of the peak currents on the scan rate for a $(PFS/PEI)_8$-PFS multilayer on ITO.

larger areas. Figure S3 (Supporting Information) shows 1 × 1 μm^2 images of $(PFS)_1$ and $(PFS/PEI)_8$-PFS films. Over this scanned area, rms roughness values for the $(PFS)_1$ and $(PFS/PEI)_8$-PFS films were 0.8 and 3.0 nm, respectively.

A cross-sectional height profile of a $(PFS/PEI)_8$-PFS film on Si had a thickness of 9.13 nm in the dry state. Ellipsometry measurements (Figure S4, Supporting Information) and the SPR results (1.4 nm/bilayer) confirmed this film thickness.

The electrochemical characteristics of the multilayers were studied by cyclic voltammetry (CV). Figure 4 shows the cyclic voltammograms corresponding to $(PFS/PEI)_n$-PFS thin films with different numbers of bilayers (n = 1, 3, 5, and 7). The double-wave voltammograms result from intermetallic coupling between the ferrocene units in the PFS chain. Because of intermetallic coupling, the oxidation potential of a ferrocene unit is increased when a neighboring ferrocene is already in the oxidized state. Therefore, ferrocene units in alternating positions along the PFS chain are oxidized first at low potential, followed by the oxidation of the remaining ferrocene units at higher potential, resulting in the double-wave voltammogram typical of PFS chains.[24c] The charge passed during oxidation and reduction increased linearly with the number of bilayers in the LbL assembly, showing that the number of ferrocene units on the surface grew linearly (Figure 4b). By the integration of the area under the redox peaks, the surface coverage of ferrocene sites for $(PFS/PEI)_7$-PFS was calculated to be 2.29 × 10^{-9} mol cm^{-2}.[41] To characterize the electroactive behavior of the redox-active assembly further, we studied the scan rate (v) dependence of the peak current (I_p), which provides powerful insight into the electrode processes that govern the redox characteristics of the film. The linear dependence of I_p on v, found for all oxidation and reduction peaks (Figure 5), is typical for surface-confined electroactive species.[41]

We investigated the stability of the multilayers in the reduced and oxidized states. In the reduced state, when held at a fixed potential of −0.1 V, the films were stable. Also, no material loss was observed after 30 CV cycles at a scan rate of 50 mV/s. After a fixed oxidizing potential of 0.6 V (vs Ag/AgCl) was maintained for 3 h, which is a rather severe test for gauging film stability, only 10% material loss occurred (Figure S5, Supporting Information). In contrast, a five-bilayer film composed of PFS polyanions and polycations (Figure S6), held together by electrostatic forces, showed much higher material losses when kept at aging potentials as low as 0.1 V.[27]

Poly(ferrocenylsilanes) are promising redox mediators with application potential in electrocatalysis and in electrochemical sensing. In previous work, we reported an ascorbic acid sensor based on a single poly(ferrocenylsilane) layer bound covalently to a gold electrode.[28] By extending this approach, we were interested in gauging the performance of the current LbL assembled films as ascorbic acid and hydrogen peroxide sensors, in particular, as a function of the number of bilayers. The amperometric response of $(PFS/PEI)_8$-PFS multilayer to ascorbic acid under an applied potential of 0.6 V (vs Ag/AgCl) was measured (Figures S7 and S8, Supporting Information). To demonstrate that the performance of electrochemical sensors based on PFS redox mediators can be enhanced by tuning the number of bilayers, we examined multilayers consisting of PFS **1** and PEI with five and nine bilayers as mediators in the electrochemical sensing of hydrogen peroxide (H_2O_2). The detection of hydrogen peroxide is of importance in pharmaceutical, clinical, environmental, textile, and food manufacturing applications.[32] It is known that at unmodified electrodes, slow electrode kinetics and high overpotential hinder the oxidation and reduction of H_2O_2 in analytical applications.[32] Figure 6 illustrates the cyclic voltammograms of

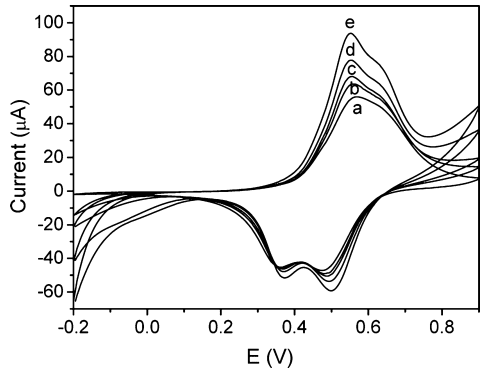

Figure 6. Cyclic voltammograms of $(PFS/PEI)_8$-PFS in the absence (a) and presence of H_2O_2 (b, 0.5; c, 1; d, 5; and e, 10 mM) at a scan rate of 50 mV/s in a 0.1 M $NaClO_4$ aqueous solution. Ag/AgCl and a Pt wire served as the reference and counter electrodes, respectively.

$(PFS/PEI)_8$-PFS in the (a) absence and (b−e) presence of H_2O_2. The peak potentials do not change, but the anodic and cathodic peak currents increase with the addition of H_2O_2, indicating that PFS mediates H_2O_2 redox processes effectively.

Figure 7 presents the sensor response of $(PFS/PEI)_4$-PFS and $(PFS/PEI)_8$-PFS multilayers to consecutive additions of H_2O_2, where its concentration increases with 25 μM incre-

dx.doi.org/10.1021/la304498g | Langmuir 2013, 29, 7257−7265

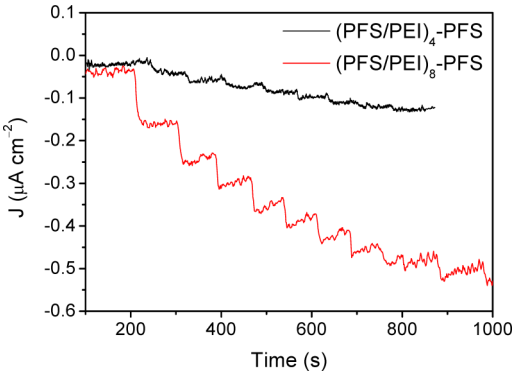

Figure 7. Amperometric responses of $(PFS/PEI)_4$-PFS and $(PFS/PEI)_8$-PFS to H_2O_2 at −0.1 V (vs Ag/AgCl) constant potential, where each step represents 25 μM H_2O_2.

ments. A very significant difference in the current densities between these multilayers is observed. Clearly, the number of accessible ferrocene moieties per unit area at the electrode directly affects the performance of the sensor. A plateau is visible in the curve of $(PFS/PEI)_4$-PFS. At the plateau, the $(PFS/PEI)_4$-PFS redox mediator is saturated by the high concentration of H_2O_2. We expect a plateau also for $(PFS/PEI)_8$-PFS; however, this may occur at higher concentrations of H_2O_2 because more redox centers are present at the electrode in the case of $(PFS/PEI)_8$-PFS.

The amperometric response of the most sensitive multilayer, $(PFS/PEI)_8$-PFS, to a smaller H_2O_2 concentration increment of 5 μM was subsequently investigated and is displayed in Figure 8a. The rapid increase in the recorded current proves that these multilayer films can detect H_2O_2 at low concentration levels. Also, these sensor layers display a fast response to H_2O_2 addition.[42] The vertical sections of the amperometric response plot (Figures 7 and 8a) indicate response times of less than 3 s. The analytical curve (R = 0.997) obtained from the chronoamperogram of $(PFS/PEI)_8$-PFS is displayed in Figure 8b. The current was found to increase linearly with H_2O_2 concentration up to 30 μM. At higher concentrations, a moderate deviation from linearity was observed. This deviation may be attributed to changes in the rate of H_2O_2 delivery to the electroactive sites. Similar deviations from linearity have been observed in the literature for other amperometric biosensors.[42−44] The limit of detection was estimated to be 3 μM at a signal-to-noise ratio of 3. It is noteworthy that the low applied working potentials (−0.1 V) used with these redox-active PFS layers are an important characteristic of interest for oxidase-based biosensors, which display poor selectivities at high applied working potentials when interfering substances are present.[45] For ascorbic acid (Figure S8), a detection limit of 1.6 μM was estimated. These detection limits match the performance of sensors reported in the literature. In the electrochemical sensing of hydrogen peroxide, sensors based on noble metal nanoparticles,[46] heme proteins and nanomaterials,[32] or porous carbon-modified electrodes[47] achieve limit of detection (LOD) values ranging from 10 to 0.1 μM, with exceptions where a LOD of 0.028 μM was demonstrated.[48] Similar to electrochemical hydrogen peroxide sensing, most of the electrochemical sensors for ascorbic acid display detection limits of between 10 [7,49,50] and 0.1 μM.[51,52]

CONCLUSIONS

This study describes the first example of a redox-active multilayer film, fabricated from a main-chain redox-active polymer (PFS) and a redox-inert polymer (PEI) interconnected by covalent bonds. The multilayer films, formed on silicon, ITO, quartz, and Au substrates by LbL deposition, were characterized by UV−vis absorption spectroscopy, FTIR, static contact angle measurements, SPR, atomic force microscopy, ellipsometry, and cyclic voltammetry, which showed that multilayer growth occurred in a well-defined manner, with the multilayer thickness increasing linearly with the number of deposited bilayers. PFS/PEI multilayers were successfully used in the electrochemical sensing of ascorbic acid and hydrogen peroxide. The efficiency of the multilayer films in these electrocatalytic processes was enhanced by increasing the number of bilayers. These layers are readily derivatized further and can therefore be regarded as a versatile platform for creating robust, tailorable redox-active interfaces.

ASSOCIATED CONTENT

Supporting Information

Photographs of solutions of the multilayer building blocks. FTIR spectra. AFM images of PFS multilayer films. Ellipsometry spectra. Graph showing PFS multilayer stability when kept at a potential of 0.6 V. Chemical structures of PFS polyions. Cyclic voltammogram and amperometric response of PFS multilayers during ascorbic acid detection. This material is available free of charge via the Internet at http://pubs.acs.org.

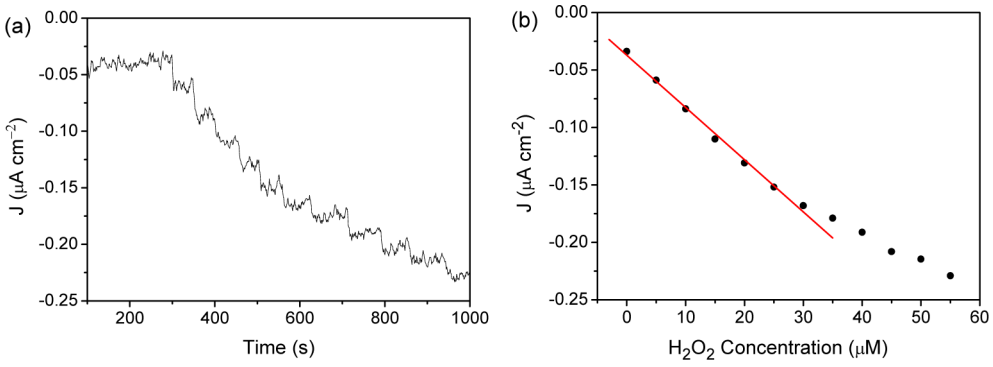

Figure 8. (a) Amperometric response of $(PFS/PEI)_8$-PFS to H_2O_2 at −0.1 V (vs Ag/AgCl) constant potential. Each step represents 5 μM H_2O_2. (b) Plot of chronoamperometric current vs H_2O_2 concentration.

dx.doi.org/10.1021/la304498g | Langmuir 2013, 29, 7257−7265

AUTHOR INFORMATION

Corresponding Author

*E-mail: g.j.vancso@utwente.nl.

Notes

The authors declare no competing financial interest.

ACKNOWLEDGMENTS

This work was financially supported by the MESA$^+$ Institute for Nanotechnology of the University of Twente and The Netherlands Organization for Scientific Research (NWO, TOP grant 700.56.322, Macromolecular Nanotechnology with Stimulus Responsive Polymers).

REFERENCES

(1) (a) Trippé, G.; Oçafrain, M.; Besbes, M.; Monroche, V.; Lyskawa, J.; Le Derf, F.; Sallé, M.; Becher, J.; Colonna, B.; Echegoyen, L. Self-Assembled Monolayers of a Tetrathiafulvalene-Based Redox-Switchable Ligand. *New J. Chem.* **2002**, *26*, 1320−1323. (b) Harris, J.; Bruening, M. Electrochemical and in Situ Ellipsometric Investigation of the Permeability and Stability of Layered Polyelectrolyte Films. *Langmuir* **2000**, *16*, 2006−2013. (c) Harris, J.; Stair, J.; Bruening, M. Layered Polyelectrolyte Films as Selective, Ultrathin Barriers for Anion Transport. *Chem. Mater.* **2000**, *12*, 1941−1946. (d) Krasemann, L.; Tieke, B. Selective Ion Transport across Self-Assembled Alternating Multilayers of Cationic and Anionic Polyelectrolytes. *Langmuir* **2000**, *16*, 287−290.

(2) Suárez-Herrera, M. F.; Costa-Figueiredo, M.; Feliu, J. M. Electrochemical and Electrocatalytic Properties of Thin Films of Poly(3,4-ethylenedioxythiophene) Grown on Basal Plane Platinum Electrodes. *Phys. Chem. Chem. Phys.* **2012**, *14*, 14391−14399.

(3) (a) Merchant, S. A.; Tran, T. O.; Meredith, M. T.; Cline, T. C.; Glatzhofer, D. T.; Schmidtke, D. W. High-Sensitivity Amperometric Biosensors Based on Ferrocene-Modified Linear Poly(ethylenimine). *Langmuir* **2009**, *25*, 7736−7742. (b) Grieshaber, D.; MacKenzie, R.; Vörös, J.; Reimhult, E. Electrochemical Biosensors−Sensor Principles and Architectures. *Sensors* **2008**, *8*, 1400−1458. (c) Harper, A.; Anderson, M. R. Electrochemical Glucose Sensors−Developments Using Electrostatic Assembly and Carbon Nanotubes for Biosensor Construction. *Sensors* **2010**, *10*, 8248−8274. (d) Ronkainen, N. J.; Halsall, H. B.; Heineman, W. R. Electrochemical Biosensors. *Chem. Soc. Rev.* **2010**, *39*, 1747−1763.

(4) (a) Willner, I.; Yan, Y.-M.; Tel-Vered, R. Integrated Enzyme-Based Biofuel Cells−A Review. *Fuel Cells* **2009**, *9*, 7−24. (b) Tamaki, T.; Ito, T.; Yamaguchi, T. Immobilization of Hydroquinone through a Spacer to Polymer Grafted on Carbon Black for a High-Surface-Area Biofuel Cell Electrode. *J. Phys. Chem. B* **2007**, *111*, 10312−10319. (c) Yu, E. H.; Scott, K. Enzymatic Biofuel Cells−Fabrication of Enzyme Electrodes. *Energies* **2010**, *3*, 23−42. (d) Meredith, M. T.; Kao, D.-Y.; Hickey, D.; Schmidtke, D. W.; Glatzhofer, D. T. High Current Density Ferrocene-Modified Linear Poly(ethylenimine) Bioanodes and Their Use in Biofuel Cells. *J. Electrochem. Soc.* **2011**, *158*, B166−B174.

(5) Willner, I.; Katz, E. Integration of Layered Redox Proteins and Conductive Supports for Bioelectronic Applications. *Angew. Chem., Int. Ed.* **2000**, *39*, 1180−1218.

(6) Eckermann, A. L.; Feld, D. J.; Shaw, J. A.; Meade, T. J. Electrochemistry of Redox-Active Self-Assembled Monolayers. *Coord. Chem. Rev.* **2010**, *254*, 1769−1802.

(7) (a) Shaidarova, L. G.; Budnikov, G. K. Chemically Modified Electrodes Based on Noble Metals, Polymer Films, or Their Composites in Organic Voltammetry. *J. Anal. Chem.* **2008**, *63*, 922−942. (b) Liu, A.; Anzai, J. Ferrocene-Containing Polyelectrolyte Multilayer Films: Effects of Electrochemically Inactive Surface Layers on the Redox Properties. *Langmuir* **2003**, *19*, 4043−4046. (c) Liu, A.; Kashiwagi, Y.; Anzai, J. Polyelectrolyte Multilayer Films Containing Ferrocene: Effects of Polyelectrolyte Type and Ferrocene Contents in the Film on the Redox Properties. *Electroanalysis* **2003**, *15*, 1139−1142. (d) Hodak, J.; Etchenique, R.; Calvo, E.; Singhal, K.; Bartlett, P. Layer-by-Layer Self-Assembly of Glucose Oxidase with a Poly(allylamine)ferrocene Redox Mediator. *Langmuir* **1997**, *13*, 2708−2716. (e) Calvo, E.; Battaglini, F.; Danilowicz, C.; Wolosiuk, A.; Otero, M. Layer-by-Layer Electrostatic Deposition of Biomolecules on Surfaces for Molecular Recognition, Redox Mediation and Signal Generation. *Faraday Discuss.* **2000**, *116*, 47−65.

(8) Calvo, E. J.; Etchenique, R.; Pietrasanta, L.; Wolosiuk, A.; Danilowicz, C. Layer-by-Layer Self-Assembly of Glucose Oxidase and $Os(Bpy)_2ClPyCH_2NH$−poly(Allylamine) Bioelectrode. *Anal. Chem.* **2001**, *73*, 1161−1168.

(9) Hervás Pérez, J. P.; López-Cabarcos, E.; López-Ruiz, B. The Application of Methacrylate-Based Polymers to Enzyme Biosensors. *Biomol. Eng.* **2006**, *23*, 233−245.

(10) Bard, A. J.; Faulkner, L. R. *Electrochemical Methods: Fundamentals and Applications*, 2nd ed.; John Wiley & Sons: New York, 2001.

(11) (a) Quinn, J. F.; Johnston, A. P. R.; Such, G. K.; Zelikin, A. N.; Caruso, F. Next Generation, Sequentially Assembled Ultrathin Films: Beyond Electrostatics. *Chem. Soc. Rev.* **2007**, *36*, 707−718. (b) *Multilayer Thin Films: Sequential Assembly of Nanocomposite Materials*, 2nd ed.; Decher, G., Schlenoff, J. B., Eds.; Wiley-VCH: Weinheim, 2012.

(12) (a) Decher, G.; Hong, J. D. Buildup of Ultrathin Multilayer Films by a Self-Assembly Process: I. Consecutive Adsorption of Anionic and Cationic Bipolar Amphiphiles on Charged Surfaces. *Makromol. Chem., Macromol. Symp.* **1991**, *46*, 321−327. (b) Decher, G.; Hong, J. D.; Schmitt, J. Buildup of Ultrathin Multilayer Films by a Self-Assembly Process: III. Consecutively Alternating Adsorption of Anionic and Cationic Polyelectrolytes on Charged Surfaces. *Thin Solid Films* **1992**, *210*, 831−835.

(13) (a) Wang, L. Y.; Wang, Z. Q.; Zhang, X.; Shen, J. C.; Chi, L. F.; Fuchs, H. A New Approach for the Fabrication of an Alternating Multilayer Film of Poly(4-vinylpyridine) and Poly(acrylic acid) Based on Hydrogen Bonding. *Macromol. Rapid Commun.* **1997**, *18*, 509−514. (b) Stockton, W. B.; Rubner, M. F. Molecular-Level Processing of Conjugated Polymers. 4. Layer-by-Layer Manipulation of Polyaniline via Hydrogen-Bonding Interactions. *Macromolecules* **1997**, *30*, 2717−2725.

(14) Guan, Y.; Zhang, Y.; Zhou, T.; Zhou, S. Stability of Hydrogen-Bonded Hydroxypropylcellulose/Poly(acrylic acid) Microcapsules in Aqueous Solutions. *Soft Matter* **2009**, *5*, 842−849.

(15) Hou, S.; Wang, J.; Martin, C. R. Template-Synthesized DNA Nanotubes. *J. Am. Chem. Soc.* **2005**, *127*, 8586−8587.

(16) Johnston, A. P. R.; Mitomo, H.; Read, E. S.; Caruso, F. Compositional and Structural Engineering of DNA Multilayer Films. *Langmuir* **2006**, *22*, 3251−3258.

(17) (a) Russell, R. J.; Sirkar, K.; Pishko, M. V. Preparation of Nanocomposite Poly(allylamine)−Poly(ethylene glycol) Thin Films Using Michael Addition. *Langmuir* **2000**, *16*, 4052−4054. (b) Such, G. K.; Quinn, J. F.; Quinn, A.; Tjipto, E.; Caruso, F. Assembly of Ultrathin Polymer Multilayer Films by Click Chemistry. *J. Am. Chem. Soc.* **2006**, *128*, 9318−9319.

(18) (a) Kohli, P.; Taylor, K. K.; Harris, J. J.; Blanchard, G. J. Assembly of Covalently-Coupled Disulfide Multilayers on Gold. *J. Am. Chem. Soc.* **1998**, *120*, 11962−11968. (b) Kohli, P.; Blanchard, G. J. Design and Growth of Robust Layered Polymer Assemblies with Molecular Thickness Control. *Langmuir* **1999**, *15*, 1418−1422. (c) Kohli, P.; Blanchard, G. J. Applying Polymer Chemistry to Interfaces: Layer-by-Layer and Spontaneous Growth of Covalently Bound Multilayers. *Langmuir* **2000**, *16*, 4655−4661. (d) Kohli, P.; Blanchard, G. J. Design and Demonstration of Hybrid Multilayer Structures: Layer-by-Layer Mixed Covalent and Ionic Interlayer Linking Chemistry. *Langmuir* **2000**, *16*, 8518−8524.

(19) (a) Schulz, C.; Nowak, S.; Fröhlich, R.; Ravoo, B. J. Covalent Layer-by-Layer Assembly of Redox Active Molecular Multilayers on Silicon (100) by Photochemical Thiol-Ene Chemistry. *Small* **2012**, *8*, 569−577. (b) El Haitami, A. E.; Thomann, J.-S.; Jierry, L.; Parat, A.; Voegel, J.-C.; Schaaf, P.; Senger, B.; Boulmedais, F.; Frisch, B.

Covalent Layer-by-Layer Assemblies of Polyelectrolytes and Homobifunctional Spacers. *Langmuir* **2010**, *26*, 12351−12357.
(20) For reviews on sequential chemical reactions, see ref 11a and the following: (a) Rydzek, G.; Schaaf, P.; Voegel, J.-C.; Jierry, L.; Boulmedais, F. Strategies for Covalently Reticulated Polymer Multilayers. *Soft Matter* **2012**, *8*, 9738−9755. (b) Such, G. K; Johnston, A. P. R; Liang, K.; Caruso, F. Synthesis and Functionalization of Nanoengineered Materials Using Click Chemistry. *Prog. Polym. Sci.* **2012**, *37*, 985−1003.
(21) Hatzor, A.; Moav, T.; Cohen, H.; Matlis, S.; Libman, J.; Vaskevich, A.; Shanzer, A.; Rubinstein, I. Coordination-Controlled Self-Assembled Multilayers on Gold. *J. Am. Chem. Soc.* **1998**, *120*, 13469−13477.
(22) Azzaroni, O.; Alvarez, M.; Abou-Kandil, A. I.; Yameen, B.; Knoll, W. Tuning the Unidirectional Electron Transfer at Interfaces with Multilayered Redox-Active Supramolecular Bionanoassemblies. *Adv. Funct. Mater.* **2008**, *18*, 3487−3496.
(23) For reviews on poly(ferrocenylsilanes) see the following: (a) Manners, I. Polymer Science with Main Group Elements and Transition Metals. *Macromol. Symp.* **2003**, *196*, 57−62. (b) Kulbaba, K.; Manners, I. Polyferrocenylsilanes: Metal-Containing Polymers for Materials Science, Self-Assembly and Nanostructure Applications. *Macromol. Rapid Commun.* **2001**, *22*, 711−724. (c) Manners, I. Poly(ferrocenylsilanes): Novel Organometallic Plastics. *Chem. Commun.* **1999**, 857−865. (d) Whittell, G. R.; Manners, I. Metallopolymers: New Multifunctional Materials. *Adv. Mater.* **2007**, *19*, 3439−3468. (e) Bellas, V.; Rehahn, M. Polyferrocenylsilane-Based Polymer Systems. *Angew. Chem., Int. Ed.* **2007**, *46*, 5082−5104. (e) *Frontiers in Transition Metal-Containing Polymers*; Abd-El-Aziz, A. S., Manners, I., Eds.; John Wiley & Sons: Hoboken, NJ, 2007.
(24) (a) Foucher, D. A.; Honeyman, C. H.; Nelson, J. M.; Tang, B. Z.; Manners, I. Organometallic Ferrocenyl Polymers Displaying Tunable Cooperative Interactions between Transition Metal Centers. *Angew. Chem., Int. Ed.* **1993**, *32*, 1709−1711. (b) Nguyen, M. T.; Diaz, A. F.; Dement'ev, V. V.; Pannell, K. H. High Molecular Weight Poly(ferrocenediyl-silanes): Synthesis and Electrochemistry of $[-(C_5H_4)Fe(C_5H_4)SiR_2-]_n$, R = Me, Et, *n*-Bu, *n*-Hex. *Chem. Mater.* **1993**, *5*, 1389−1394. (c) Rulkens, R.; Lough, A. J.; Manners, I.; Lovelace, S. R.; Grant, C.; Geiger, W. E. Linear Oligo(ferrocenyldimethylsilanes) with between Two and Nine Ferrocene Units: Electrochemical and Structural Models for Poly(ferrocenylsilane) High Polymers. *J. Am. Chem. Soc.* **1996**, *118*, 12683−12695. (d) Péter, M.; Lammertink, R. G. H.; Hempenius, M. A.; Vancso, G. J. Electrochemistry of Surface-Grafted Stimulus-Responsive Monolayers of Poly(ferrocenyldimethylsilane) on Gold. *Langmuir* **2005**, *21*, 5115−5123.
(25) (a) Hempenius, M. A.; Robins, N. S.; Péter, M.; Kooij, E. S.; Vancso, G. J. Water-Soluble Poly(ferrocenylsilanes) for Supramolecular Assemblies by Layer-by-Layer Deposition. *Langmuir* **2002**, *18*, 7629−7634. (b) Ginzburg, M.; Galloro, J.; Jäkle, F.; Power-Billard, K. N.; Yang, S.; Sokolov, I.; Lam, C. N. C.; Neumann, A. W.; Manners, I.; Ozin, G. A. Layer-by-Layer Self-Assembly of Organic−Organometallic Polymer Electrostatic Superlattices Using Poly(ferrocenylsilanes). *Langmuir* **2000**, *16*, 9609−9614. (c) Halfyard, J.; Galloro, J.; Ginzburg, M.; Wang, Z.; Coombs, N.; Manners, I.; Ozin, G. A. Direct Visualization of Layer-by-Layer Self-Assembled Multilayers of Organometallic Polymers. *Chem. Commun.* **2002**, 1746−1747.
(26) (a) Ma, Y.; Dong, W.-F.; Hempenius, M. A.; Möhwald, H.; Vancso, G. J. Redox-Controlled Molecular Permeability of Composite-Wall Microcapsules. *Nat. Mater.* **2006**, *5*, 724−729. (b) Ma, Y.; Dong, W.-F.; Kooij, E. S.; Hempenius, M. A.; Möhwald, H.; Vancso, G. J. Supramolecular Assembly of Water-Soluble Poly(ferrocenylsilanes): Multilayer Structures on Flat Interfaces and Permeability of Microcapsules. *Soft Matter* **2007**, *3*, 889−895.
(27) Song, J.; Jańczewski, D.; Ma, Y.; Hempenius, M. A.; Xu, J.; Vancso, G. J. Redox-Controlled Release of Molecular Payloads from Multilayered Organometallic Polyelectrolyte Films. *J. Mater. Chem. B* **2013**, *1*, 828−834.
(28) Sui, X. F.; Feng, X. L.; Song, J.; Hempenius, M. A.; Vancso, G. J. Electrochemical Sensing by Surface-Immobilized Poly(ferrocenylsilane) Grafts. *J. Mater. Chem.* **2012**, *22*, 11261−11267.
(29) For PFS chains tethered by their chain ends to electrodes, see the following: (a) Péter, M.; Lammertink, R. G. H.; Hempenius, M. A.; van Os, M.; Beulen, M. W. J.; Reinhoudt, D. N.; Knoll, W.; Vancso, G. J. Synthesis, Characterization and Thin Film Formation of End-Functionalized Organometallic Polymers. *Chem. Commun.* **1999**, 359−360. (b) Péter, M.; Hempenius, M. A.; Kooij, E. S.; Jenkins, T. A.; Roser, S. J.; Knoll, W.; Vancso, G. J. Electrochemically Induced Morphology and Volume Changes in Surface-Grafted Poly(ferrocenyldimethylsilane) Monolayers. *Langmuir* **2004**, *20*, 891−897. (c) Zou, S.; Ma, Y.; Hempenius, M. A.; Schönherr, H.; Vancso, G. J. Grafting of Single, Stimuli-Responsive Poly(ferrocenylsilane) Polymer Chains to Gold Surfaces. *Langmuir* **2004**, *20*, 6278−6287.
(30) Tam, T. K.; Zhou, J.; Pita, M.; Ornatska, M.; Minko, S.; Katz, E. Biochemically Controlled Bioelectrocatalytic Interface. *J. Am. Chem. Soc.* **2008**, *130*, 10888−10889.
(31) Zhang, S.; Yang, W.; Niu, Y.; Sun, C. Multilayered Construction of Glucose Oxidase and Poly(allylamine)ferrocene on Gold Electrodes by means of Layer-by-Layer Covalent Attachment. *Sens. Actuators B* **2004**, *101*, 387−393.
(32) Chen, W.; Cai, S.; Ren, Q.-Q.; Wen, W.; Zhao, Y.-D. Recent Advances in Electrochemical Sensing for Hydrogen Peroxide: A Review. *Analyst* **2012**, *137*, 49−58.
(33) Hempenius, M. A.; Brito, F. F.; Vancso, G. J. Synthesis and Characterization of Anionic and Cationic Poly(ferrocenylsilane) Polyelectrolytes. *Macromolecules* **2003**, *36*, 6683−6688.
(34) Kooij, E. S.; Ma, Y.; Hempenius, M. A.; Vancso, G. J.; Poelsema, B. Optical Properties of Poly(ferrocenylsilane) Multilayer Thin Films. *Langmuir* **2010**, *26*, 14177−14181.
(35) Erol, M.; Du, H.; Sukhishvili, S. Control of Specific Attachment of Proteins by Adsorption of Polymer Layers. *Langmuir* **2006**, *22*, 11329−11336.
(36) Manners, I. Ring-Opening Polymerization of Metallocenophanes: A New Route to Transition Metal-Based Polymers. *Adv. Organometal. Chem.* **1995**, *37*, 131−168.
(37) Bertrand, P.; Jonas, A.; Laschewsky, A.; Legras, R. Ultrathin Polymer Coatings by Complexation of Polyelectrolytes at Interfaces: Suitable Materials, Structure and Properties. *Macromol. Rapid Commun.* **2000**, *21*, 319−348.
(38) (a) Kesim, H.; Rzaev, Z. M. O.; Dinçer, S.; Pişkin, E. Functional Bioengineering Copolymers. II. Synthesis and Characterization of Amphiphilic Poly(*N*-isopropyl Acrylamide-*co*-Maleic Anhydride) and its Macrobranched Derivatives. *Polymer* **2003**, *44*, 2897−2909. (b) Stewart, J. E. Vibrational Spectra of Primary and Secondary Aliphatic Amines. *J. Chem. Phys.* **1959**, *30*, 1259−1265. (c) Daniel, M. F.; Desbat, B.; Cruege, F.; Trinquet, O.; Lassegues, J. C. Solid State Protonic Conductors: Poly(ethylene imine) Sulfates and Phosphates. *Solid State Ionics* **1988**, *28*−*30*, 637−641.
(39) Yoo, D.; Shiratori, S. S.; Rubner, M. F. Controlling Bilayer Composition and Surface Wettability of Sequentially Adsorbed Multilayers of Weak Polyelectrolytes. *Macromolecules* **1998**, *31*, 4309−4318.
(40) (a) Buck, M. E.; Schwartz, S. C.; Lynn, D. M. Superhydrophobic Thin Films Fabricated by Reactive Layer-by-Layer Assembly of Azlactone-Functionalized Polymers. *Chem. Mater.* **2010**, *22*, 6319−6327. (b) Tan, Q.; Ji, J.; Barbosa, M. A.; Fonseca, C.; Shen, J. Constructing Thromboresistant Surface on Biomedical Stainless Steel via Layer-by-Layer Deposition Anticoagulant. *Biomaterials* **2003**, *24*, 4699−4705.
(41) (a) Murray, R. W. In *Electroanalytical Chemistry*; Bard, A. J., Ed.; Marcel Dekker: New York, 1984; Vol. *13*, p 191. (b) Finkley, H. O. In *Electroanalytical Chemistry*; Bard, A. J., Rubinstein, I., Eds.; Marcel Dekker: New York, 1996; Vol. *19*, p 109.
(42) Tripathi, V. S.; Kandimalla, V. B.; Ju, H. Amperometric Biosensor for Hydrogen Peroxide Based on Ferrocene-Bovine Serum Albumin and Multiwall Carbon Nanotube Modified Ormosil Composite. *Biosens. Bioelectron.* **2006**, *21*, 1529−1535.

(43) Razmi, H.; Harasi, M. Voltammetric Behavior and Amperometric Determination of Ascorbic Acid at Cadmium Pentacyanonitrosylferrate Film Modified GC Electrode. *Int. J. Electrochem. Sci.* **2008**, *3*, 82−95.
(44) Zhang, Z. B.; Yuan, S. J.; Zhu, X. L.; Neoh, K. G.; Kang, E. T. Enzyme-Mediated Amperometric Biosensors Prepared via Successive Surface-Initiated Atom-Transfer Radical Polymerization. *Biosens. Bioelectron.* **2010**, *25*, 1102−1108.
(45) Schuvailo, O. M.; Gáspár, S.; Soldatkin, A. P.; Csöregi, E. Ultramicrobiosensor for the Selective Detection of Glutamate. *Electroanalysis* **2007**, *19*, 71−78.
(46) Wang, J. Electrochemical Biosensing Based on Noble Metal Nanoparticles. *Microchim. Acta* **2012**, *177*, 245−270.
(47) Walcarius, A. Electrocatalysis, Sensors and Biosensors in Analytical Chemistry Based on Ordered Mesoporous and Macroporous Carbon-Modified Electrodes. *Trends Anal. Chem.* **2012**, *38*, 79−97.
(48) Fei, J. J.; Jia, S. S.; Tian, T.; Zhou, F. Q. Reagentless Biosensor for Hydrogen Peroxide Based on the Immobilization of Hemoglobin in Platinum Nanoparticles Enhanced Poly(chloromethyl thiirane) Cross-Linked Chitosan Hybrid Film. *Electroanalysis* **2009**, *21*, 1424−1431.
(49) Weng, C.-J.; Jhuo, Y.-S.; Chen, Y.-L.; Feng, C.-F.; Chang, C.-H.; Chen, S.-W.; Yeh, J.-M.; Wei, Y. Intrinsically Electroactive Polyimide Microspheres Fabricated by Electrospraying Technology for Ascorbic Acid Detection. *J. Mater. Chem.* **2011**, *21*, 15666−15672.
(50) Wang, S.; Du, D. Differential Pulse Voltammetry Determination of Ascorbic Acid with Ferrocene-L-Cysteine Self-Assembled Supramolecular Film Modified Electrode. *Sens. Actuators, B* **2004**, *97*, 373−378.
(51) Shahrokhian, S.; Zare-Mehrjardi, H. R. Simultaneous Voltammetric Determination of Uric Acid and Ascorbic Acid Using a Carbon-Paste Electrode Modified with Multi-Walled Carbon Nanotubes/Nafion and Cobalt(II)nitrosalophen. *Electroanalysis* **2007**, *19*, 2234−2242.
(52) Malinauskas, A.; Garjonytė, R.; Mažeikienė, R.; Jurevičiūtė, I. Electrochemical Response of Ascorbic Acid at Conducting and Electrogenerated Polymer Modified Electrodes for Electroanalytical Applications: A Review. *Talanta* **2004**, *64*, 121−129.